

Prodrug based on halloysite delivery systems to improve the antitumor ability of methotrexate in leukemia cell lines

Marina Massaro,^{a,1} Paola Poma,^{a,1} Giuseppe Cavallaro,^b Fátima García-Villén,^c Giuseppe Lazzara,^b Monica Notarbartolo di Villarosa,^a Nicola Muratore,^b Rita Sánchez-Espejo,^c Cesar Viseras Iborra,^{c,d} and Serena Riela^{a,}*

^aDipartimento di Scienze Biologiche, Chimiche e Farmaceutiche (STEBICEF), University of Palermo Viale delle Scienze, 90128 Palermo, Italy. E-mail: serena.riela@unipa.it

^bDipartimento di Fisica e Chimica “E. Segrè (DiFC), University of Palermo, Viale delle Scienze, 90128 Palermo, Italy

^cConsorzio Interuniversitario Nazionale per la Scienza e Tecnologia dei Materiali, INSTM, I-50121 Firenze, Italy

^eDepartment of Pharmacy and Pharmaceutical Technology, Faculty of Pharmacy, University of Granada, Campus of Cartuja, 18071 s/n, Granada, Spain

^dAndalusian Institute of Earth Sciences, CSIC-UGR, Avenida de las Palmeras 4, 18100, Armilla, Granada, Spain

¹Contributed equally

KEYWORDS. Halloysite nanotubes, methotrexate, prodrug, biotin, drug delivery systems, leukemia cells.

ABSTRACT. The prodrug approach, as well as the development of specific systems able to deliver a chemotherapeutic agent in the target site, decreasing the side effects often associated with its administration, are still a challenging. In this context, both methotrexate drug molecules (MTX) and biotin ligand moieties, whose receptors are overexpressed on the surface of several cancer

cells, were loaded on halloysite nanotubes (HNTs) to develop nanomaterial based on multifunctional and “smart” delivery systems.

To highlight the crucial role played by biotin, carrier systems based on HNTs and MTX were also synthesized. In detail, several approaches were envisaged: *i*) a supramolecular interaction between the clay and the drug; *ii*) a covalent grafting of the drug onto the HNTs external surface and, *iii*) a combination of both approaches. The nanomaterials obtained were characterized by thermogravimetric analysis, FT-IR, and UV-*vis* spectroscopies, DLS and ζ -potential measurements and the morphologies were imaged by HAADF/STEM investigations. Kinetic release experiments at different pH conditions were also performed. Finally, as a proof-of-concept application of our pro-drug delivery systems based on HNTs in cancer therapy, the cytotoxic effects were evaluated on acute myeloid leukemia cell lines, HL60 and its multidrug resistance variant, HL60R. The obtained results showed that both the MTX prodrug system and the biotinylated ones played a crucial role in the biological activity and, they are promising agents for the cancer treatments.

1.Introduction

Up to now, cancer is still one of the main causes of death over the world. Although surgery and radiotherapy are the most effective treatments for non-metastatic cancers, the development of innovative treatments to contrast the metastatic ones represents a challenge in the healthcare field. Methotrexate (MTX) is as an antimetabolite agent, which inhibits the dihydrofolate reductase receptors preventing the cell division and proliferation by the inhibition of the synthesis of the nucleoside thymidine.¹ In addition, it has been demonstrated that MTX can be efficiently taken up by tumor cells,² since it is structurally similar to folic acid, the target molecule for dihydrofolate reductase receptors.

Although MTX has good antitumor activity, its applications are greatly limited due to the short half-life, poor water solubility, low bioavailability, drug resistance, and, several side effects which hindered its clinical efficacy;³⁻⁵ furthermore, MTX cannot discriminate between healthy and cancer cells. For these reasons, its clinical uses are often limited.

The prodrug approach, that aims to improve the properties of drugs, their solubility and decrease their toxicity, has been one of the most promising means of site-specific drug delivery.⁶ Amide is one of the major chemical groups employed to link carrier directly to the drug.⁷ Carriers designated in this approach should have some characteristics such as: adequate functional groups for chemical

fixation of the drug, high stability, loading capacity, be biodegradable, low intrinsic toxicity, show very low accumulation in the body, and keep the activity of the delivered drug, until it reaches the site of action.

Clay minerals possessing interesting properties such as high biocompatibility, suitable particle size and morphology and specific surface area, represent since ancient times nanomaterials that can be safely used in medicine.⁸

Recently, halloysite nanotubes (HNTs), a clay mineral belonging to the kaolin group, have attracted attention for use in cancer treatment due to their peculiar structure and properties.

HNTs are an aluminosilicate clay with a predominantly hollow tubular structure and chemically similarly to the platy kaolinite ($\text{Al}_2\text{Si}_2\text{O}_5(\text{OH})_4 \cdot n\text{H}_2\text{O}$). Generally, the length of the tubes is in the range of 0.2–1.5 μm , while their inner and outer diameters are in the ranges of 10–30 nm and 40–70 nm, respectively.⁹ HNTs, naturally occurring in huge quantities at low cost, show excellent biocompatibility.^{10–11} Halloysite is positively charged in the inner lumen, which consists mostly of aluminum hydroxide, whereas the external surface, which is silicon dioxide,¹³ is negatively charged. The different surface chemistry allows the selective functionalization at the inner and/or outer side making possible the synthesis of several nanomaterials with hierarchical nanostructure^{8, 14–15} which found applications in several fields.^{16–20} Most importantly, HNTs are able to penetrate the cellular membrane surrounding the cell nuclei.^{21–22} In addition, it has been proved that the modification of the tubes surfaces makes hybrid nanomaterials that penetrate the nucleus membrane, as well.²³

There are many examples of the use of pristine HNTs as carrier for biological active molecules in which the drug molecules are supramolecular loaded, by hydrogen bonding or electrostatically or hydrophobic interactions with the tubes; but only few examples of them are about the covalent linkage between HNTs and drug to form a prodrug based on HNTs nanomaterial. In this context, we showed that the dual-stimuli-responsive halloysite-curcumin prodrug dramatically enhanced the release of the drug from the carrier as well as its cytotoxicity activity, increasing its stability under acidic condition and retained its physico-chemical properties.²⁴

Herein, to improve the pharmacological activity of MTX by reducing some of its side effects, we synthesized and characterized different systems based on halloysite nanotubes and MTX by exploiting different approaches. In detail, we envisaged: *i*) a supramolecular interaction between

the clay and the drug; *ii*) a covalent grafting of the drug onto the HNTs external surface and, *iii*) a combination of both approaches.

In addition, to reduce systemic toxic effects, to enhance the cellular uptake and to increase the therapeutic efficacy of the MTX in cancer cells, an active targeting system the surface receptor-mediated drug delivery system strategy was developed.²⁵

Among the different molecules which serve to this scope, biotin, as an essential micronutrient for cell proliferation, is a good, targeted ligand due to the over expression of its receptors in many cancer cells, whereas the receptors are rarely expressed in normal cells.²⁶ The strong and specific interaction between biotin and biotin receptors could facilitate the receptor-mediated endocytosis of biotinylated nanoparticles in cancer cells.²⁷⁻²⁹

Recently D. Mills *et al.*³⁰ loaded, by a supramolecular approach, both MTX and folic acid, ligand able to interact with folate receptor present on the surface of cells. The resulting nanomaterial showed a selective target cancer cell as well as a dramatically reduction of the side effects of the drug. In that respect, herein we report modified HNTs with covalently linked biotin moieties, that should be a promising tool to develop nanomaterial based on multifunctional and “smart” delivery systems. The covalent linkage of biotin instead of its supramolecular binding the was chosen to make use of the major advantages of this approach, in particular the great stability of the hybrid material, the control over the degree of functionalization, and the data reproducibility. All nanomaterials obtained were characterized by several techniques and their morphology was investigated by HAADF/STEM measurements and the kinetic release was also investigated.

Finally, as a proof-of-concept application of our drug delivery systems based on HNTs in cancer therapy, the cytotoxic effects of the multifunctional carriers were evaluated on acute myeloid leukemia cell lines, HL60 and its multidrug resistance variant, HL60-R, obtained with increasing doses of doxorubicin and characterized by constitutive expression of the transcription factor NF- κ B, overexpression of P-glycoprotein and inhibitor of apoptosis proteins (IAPs).³¹

MATERIALS AND METHODS. All chemicals were obtained from Sigma-Aldrich and used as received. Halloysite (Merck) was used as purchased without further purification. It presented an average tube diameter of 50 nm and inner lumen diameter of 15 nm. Typical specific surface area is 65 m² g⁻¹; pore volume of ~1.25 cm³ g⁻¹; refractive index 1.54 and specific gravity 2.53 g cm⁻³. FT-IR spectra (KBr) were recorded with an Agilent Technologies Cary 630 FT-IR spectrometer. Specimens for these measurements were prepared by mixing 5 mg of the sample powder with 100

mg of KBr. Thermogravimetric (TG) analyses were carried out through a Q5000 IR apparatus (TA Instruments) under nitrogen atmosphere (gas flows of 25 and 10 cm³ min⁻¹ were employed for the sample and the balance, respectively). The experiments were carried out by heating the sample (ca. 5 mg) to 800 °C. The heating rate was 20 °C min⁻¹. UV–vis measurements were performed using a Beckmann DU 650 spectrometer. The dispersions were sonicated with a FALC Instruments ultrasound bath at power of 180 W, stirred with a VELP Scientifica magnetic stirrer and evacuated with a rotavapor® Buchi. Powders were dried in a Buchi glass oven B-585. Transmission electron microscopy (TEM) was performed by means of a FEI Titan G2 60–300 ultra-high-resolution transmission electron microscope (FEI, Lausanne, Switzerland) coupled with analytical electron microscopy (AEM) performed with a SUPER X silicon drift windowless energy dispersive X-ray spectroscopy (XEDS) detector. AEM spectra were saved in mode STEM (scanning transmission electron microscopy) with a HAADF (high angle annular dark field) detector. X-ray chemical element maps were also collected. Zetasizer Nano-ZS (Malvern Instruments) apparatus was employed to perform Dynamic light scattering (DLS) and ζ - potential measurements. Both experiments were conducted on aqueous dispersions (concentration = 10⁻³ wt%) at 25.0 ± 0.1 °C. As concerns DLS investigations, the wavelength and the scattering angle were set at 632.8 nm and 173°, respectively. The registered field-time autocorrelation functions were analyzed by using an Inverse La Place transformation. The HPLC was performed by means of an Agilent model 1260 infinity, with degaser G4225A, binary pump G1312B, auto sampler G1329B, thermostated column compartment G1316A equipped with a multi-channel UV-vis spectrophotometric detector (DAD) G4212A. The column used was a Zorbax SB-C18 (dimensions 2.1 x 50 mm, particle diameter 1.8 µm) having a stationary phase in porous silica modified with octadecyl silane chemically bonded functionality. The method settings were as follows: sample injection volume 5 µL; eluent flow rate 0.6 mL min⁻¹; column temperature 303.15 K; eluent composition: water with 0.1% formic acid/acetonitrile with 0.1% formic acid (87%:13%); detection wavelength 305 nm. Acetonitrile (HiPerSolv CHROMANORM® for HPLC - SUPER GRADIENT Reag. Ph. Eur., USP, ACS water < 30 ppm - suitable for UPLC/UHPLC), Water (HiPerSolv CHROMANORM® for HPLC) and Formic Acid (Fluka, eluent additive for LC-MS) were used. The method of MTX quantification involve: *i*) direct injection of a small volume of sample; *ii*) chromatographic separation of MTX; *iii*) integration of the MTX chromatographic peak (retention time 0.74 min). Various solution at

different MTX concentrations were used for calibration. **HNTs-2** was prepared as reported elsewhere.³²

2.1. Synthesis of HNTs-1

To a dispersion of pristine HNTs in H₂O (5 mL), 1 mL of a solution 10⁻² M of MTX in MeOH/DMSO (1:1) was added. The suspension was sonicated for 5 min, at an ultrasound power of 200 W and at 25 °C and then was evacuated for 3 cycles. The suspension was left under stirring for 18 h at room temperature. After this time, the powder was washed with water, until the unreacted MTX was removed and, then dried at 60 °C under vacuum.

2.2. Synthesis of HNTs-3

MTX (50 mg, 0.12 mmol) was suspended in DMF (10 mL), and 1-Ethyl-3-(3'-dimethylaminopropyl)carbodiimide (EDC HCl) (35 mg, 0.15 mmol) was added. The suspension was stirred under an argon atmosphere at room temperature for 10 min. Then, **HNTs-2** (100 mg) was quickly added. The mixture was stirred for 48 h. Then, the solvent was removed by filtration; the powder was then rinsed successively with H₂O and CH₂Cl₂ and finally dried at 80 °C under vacuum.

2.3. Synthesis of HNTs-4

To a dispersion of **HNTs-3** in H₂O (5 mL), 1 mL of a solution 10⁻² M of MTX in MeOH/DMSO (1:1) was added. The suspension was sonicated for 5 min, at an ultrasound power of 200 W and at 25 °C and then was evacuated for 3 cycles. The suspension was left under stirring for 18 h at room temperature. After this time, the powder was washed with water, until the unreacted MTX was removed and, then dried at 60 °C under vacuum.

2.4. Synthesis of HNTs-5

Biotin (30 mg, 0.12 mmol) was suspended in DMF (10 mL), and 1-Ethyl-3-(3'-dimethylaminopropyl)carbodiimide (EDC HCl) (35 mg, 0.15 mmol) was added. The suspension was stirred under an argon atmosphere at room temperature for 10 min. Then, **HNTs-2** (100 mg) was quickly added. The mixture was stirred for 48 h. Then, the solvent was removed by filtration;

the powder was then rinsed successively with H₂O and CH₂Cl₂ and finally dried at 80 °C under vacuum.

2.5. Synthesis of HNTs-6

MTX (50 mg, 0.12 mmol) was suspended in DMF (10 mL), and 1-Ethyl-3-(3'-dimethylaminopropyl)carbodiimide (EDC HCl) (35 mg, 0.15 mmol) was added. The suspension was stirred under an argon atmosphere at room temperature for 10 min. Then, **HNTs-5** (100 mg) was quickly added. The mixture was stirred for 48 h. Then, the solvent was removed by filtration; the powder was then rinsed successively with H₂O and CH₂Cl₂ and finally dried at 80 °C under vacuum.

2.6. Synthesis of HNTs-7

To a dispersion of **HNTs-5** in H₂O (5 mL), 1 mL of a solution 10⁻² M of MTX in MeOH/DMSO (1:1) was added. The suspension was sonicated for 5 min, at an ultrasound power of 200 W and at 25 °C and then was evacuated for 3 cycles. The suspension was left under stirring for 18 h at room temperature. After this time, the powder was washed with water, until the unreacted MTX was removed and, then dried at 60 °C under vacuum.

2.7. Kinetic Release

The release of MTX from the different HNTs nanomaterials was done as follows: 20 mg of the sample were dispersed in 1 mL of dissolution medium (HCl 1·10⁻³ M and phosphate buffers pH 7.4) and transferred into a sealed dialysis membrane (Medicell International Ltd MWCO 12-14000 Da with a diameter of 21.5 mm). Subsequently the membrane was put in a round bottom flask containing 9 mL of the release medium, maintained at 37 °C under constant stirring. At fixed time, 1 mL of the release medium has been withdrawn and analyzed by HPLC measurements. To ensure sink conditions, 1 mL of fresh solution has been used to replace the collected one.

Total amounts of drug released (F_t) were calculated as follows:

$$F_t = V_m C_t + \sum_{i=0}^{t-1} V_a C_i \quad (\text{Eq. 1})$$

where V_m and C_t are the volume and the concentration of the drug at time t . V_a is the volume of the sample withdrawn and C_i is the drug concentration at time i ($i < t$).

The kinetics of MTX release from the different platforms have been studied by fitting the curves to different theoretical models: first order, Korsmeyer-Peppas (power law) and, the correlation coefficient (R^2) was used to describe the goodness-of-fit of each model to the experimental data.

2.8. Cell lines and Cell growth assays

The HL-60 cells were obtained from ATCC®(CCL-240, Rockville, MD, USA), while its variant HL-60R were cultured as previously described.³³

The cell lines were cultured in Roswell Park Memorial Institute (RPMI) 1640, (HyClone Europe Ltd., Cramlington, UK) supplemented with 10% heat-inactivated fetal calf serum, 2 mM L-glutamine, 100 units/mL penicillin and 100 μ g/mL streptomycin (all reagents were from HyClone Europe Ltd., Cramlington, UK) in a humidified atmosphere at 37 °C in 5% CO₂.

The cells were seeded at 5×10^3 cells/well onto 96-well plates and incubated overnight at 37 °C. At time 0, the medium was replaced with fresh complete medium supplemented with the synthesized nanomaterials. Following 72 h of treatment, 15 μ L commercial solution obtained from Promega Corp. (Madison, WI, USA) containing 3-(4,5-dimethylthiazol-2-yl)-5-(3-carboxymethoxyphenyl)-2-(4-sulphophenyl)-2H-tetrazolium (MTS) and phenazine ethosulfate was added. The plates were incubated in a humidified atmosphere at 37 °C in 5% CO₂ for 2 h, and the bioreduction of MTS dye was evaluated by measuring the absorbance of each well at 490 nm using a microplate absorbance reader (iMark Microplate Reader; Bio-Rad Laboratories, Inc., Hercules, CA, USA). Cell growth inhibition was expressed as a percentage of the absorbance of the control cells.

3. Results and Discussion

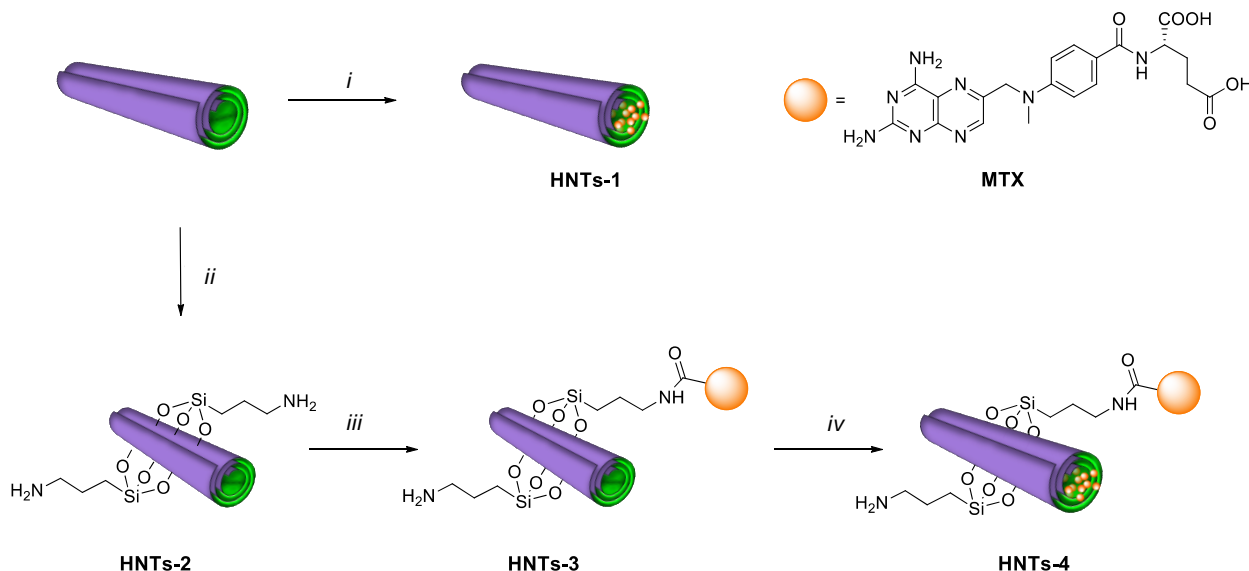
One of the most important characteristics of pristine HNTs is the formation of an inclusion complex by interaction of their internal surface with a variety of drug molecules. In addition, the free hydroxyl groups present at the external surface on the nanotubes could be used for the covalent coupling of targeting moieties and/or cytotoxic drugs. In this way, taking advantage of both the morphology and the chemical composition of halloysite different approaches were envisaged to obtain MTX carrier or delivery systems based on HNTs nanomaterials: *i*) a supramolecular

interaction between the clay and the drug; *ii*) a covalent grafting of the drug onto the HNTs external surface and, *iii*) a combination of both approaches.

Trying to overcome the multidrug resistance often associated with the use of MTX as drug, we also modified HNTs to obtain delivery systems using as targeting molecule the biotin one.

3.1. HNTs-MTX prodrug systems

Firstly, the MTX was supramolecular loaded onto the HNTs lumen according to the common adopted experimental procedure for drugs inclusion into HNTs; namely by mixing an aqueous dispersion of HNTs with a highly concentrated MTX solution (MeOH/DMSO 1:1) (Scheme 1).



Scheme 1. Schematic representation of the synthesis of **HNTs-1** and **HNTs-3** nanomaterials. Synthetic route: (i) 3-APTMS, toluene, 110 °C, 30 h; (ii) MTX, H₂O, vacuum, 18 h, r.t., (iii) MTX, EDC·HCl, DMF, 48 h, r.t., (iv) MTX, H₂O, vacuum, 18 h, r.t..

Then, the obtained suspension was stirred and maintained under vacuum for 3 to 5 min, resulting in light fizzling, which indicated that air was being removed from the tubes. Once the vacuum was removed, the solution entered the lumen, and the loaded compound condensed within the tubes. This procedure was repeated 2 to 3 times to improve the loading efficiency. After loading, the **HNTs-1** nanomaterial was washed with water to remove free MTX molecules. The drug loading of **HNTs-1** was estimated by HPLC measurements. The amount of MTX loaded in the HNTs

nanomaterial, expressed as the percent amount of drug in the final composite, was ca. 5 wt % (50 mg g⁻¹) with an entrapment efficiency of 99.4%.

The synthesis of **HNTs-3** prodrug was achieved by covalent grafting of MTX on **HNTs-2** nanomaterial in DMF, using EDC as coupling agent, at room temperature for 4 days. After work-up the amount of MTX linked onto HNTs, as estimated by TGA, was ca. 4 wt% with a degree of functionalization of 0.08 mmol g⁻¹. Based on these findings we determined that the mole ratio between MTX and the amino groups linked onto HNTs surface was 1:6. It is worth to note that complete linkage of MTX on HNTs surface is not achieved probably due to steric hindrance. The presence of some unreacted amino groups still present onto HNTs could be useful both for further modifications and to improve cellular uptake.

Afterwards, trying to increase the MTX amount on the nanomaterials, **HNTs-3** prodrug was further loaded, by adopting the same experimental procedure described above, with MTX affording the final nanomaterial **HNTs-4** prodrug (Scheme 1) with a ca. 4 wt% of drug loaded onto the system. Figure 1 compares the thermogravimetric curves of the modified HNTs with those of pure MTX and HNTs. As shown in Figure 1a, the residual mass at 700 °C (MR700) of MTX is negligible indicating that the thermal degradation of the molecule was complete. It should be noted that three different degradation steps are observed for MTX within the ranges 25-150 °C, 200-350 °C and 500-700 °C. Figure 1b highlights that **HNTs-1** presents a lower MR700 value (75.5 %) compared to pure HNTs (82.2%) due to the MTX loading. In addition, the mass loss up to 150 °C (ML150) is reduced in the loaded HNTs indicating a decrease of the halloysite hydrophilicity. Figure 1c compares the thermogravimetric curves for **HNTs-2**, **HNTs-3**, and **HNTs-4**. We observed that **HNTs-2** and **HNTs-3** present lower MR700 values (81.7 and 77.7%) with respect to that of halloysite as a consequence of the covalent grafting on the halloysite outer surface. A further MR700 decrease (72.5%) was detected in the **HNTs-4** sample that is consistent with the successful MTX loading. Interestingly, the **HNTs-4** sample shows two separate mass losses in the range between 200 and 350 °C that could be attributed to the degradation of two fractions of MTX (the loaded and the covalent grafted ones).

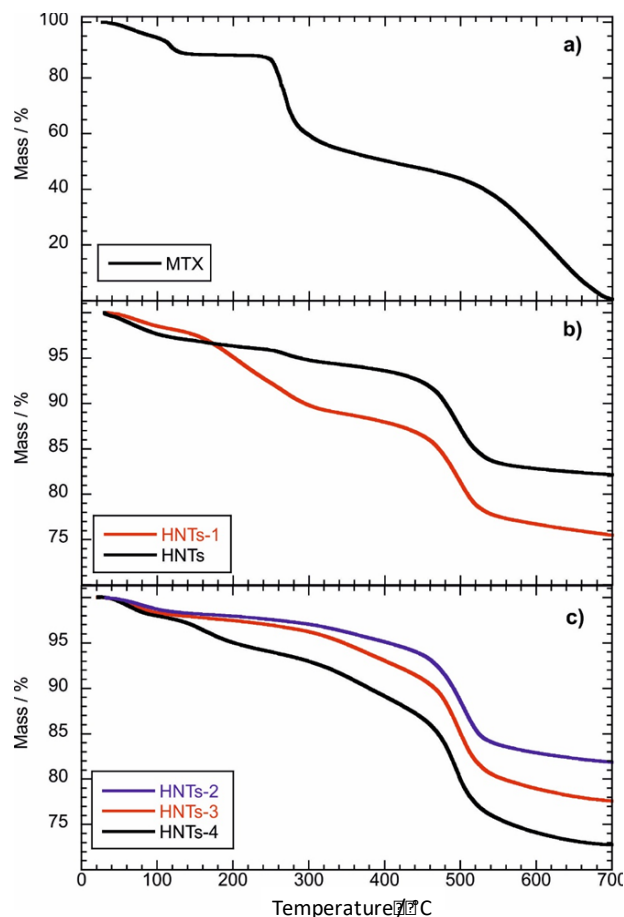


Figure 1. Thermogravimetric curves of (a) MTX; (b) HNTs and **HNTs-1**; (c) **HNTs-2**, **HNTs-3** and, **HNTs-4**.

Furthermore, the **HNTs-1** and **HNTs-3** nanomaterials were characterized by means of FT-IR spectroscopy (Figure 2a-b). The spectroscopic study showed that both nanomaterials present, in their FT-IR spectra the typical HNTs vibration stretching bands. The FT-IR spectra of both **HNTs-1** and **HNTs-3** show, beside the HNTs bands, some stretching bands related to the drug.³⁴ In particular, the band at ca. 2980 and 2850 cm^{-1} related to stretching of methylene groups, the band at ca. 1650 cm^{-1} which superimposed the typical band of HNTs, due to the stretching of the amide C=O and the bands around 1483 and 1435 cm^{-1} due to the stretching of the C–N groups. Furthermore, in the **HNTs-3** FT-IR spectrum (Figure 2b), it is also possible to observe the band at ca. 3320 cm^{-1} related to stretching of the N–H group of the amide bond.

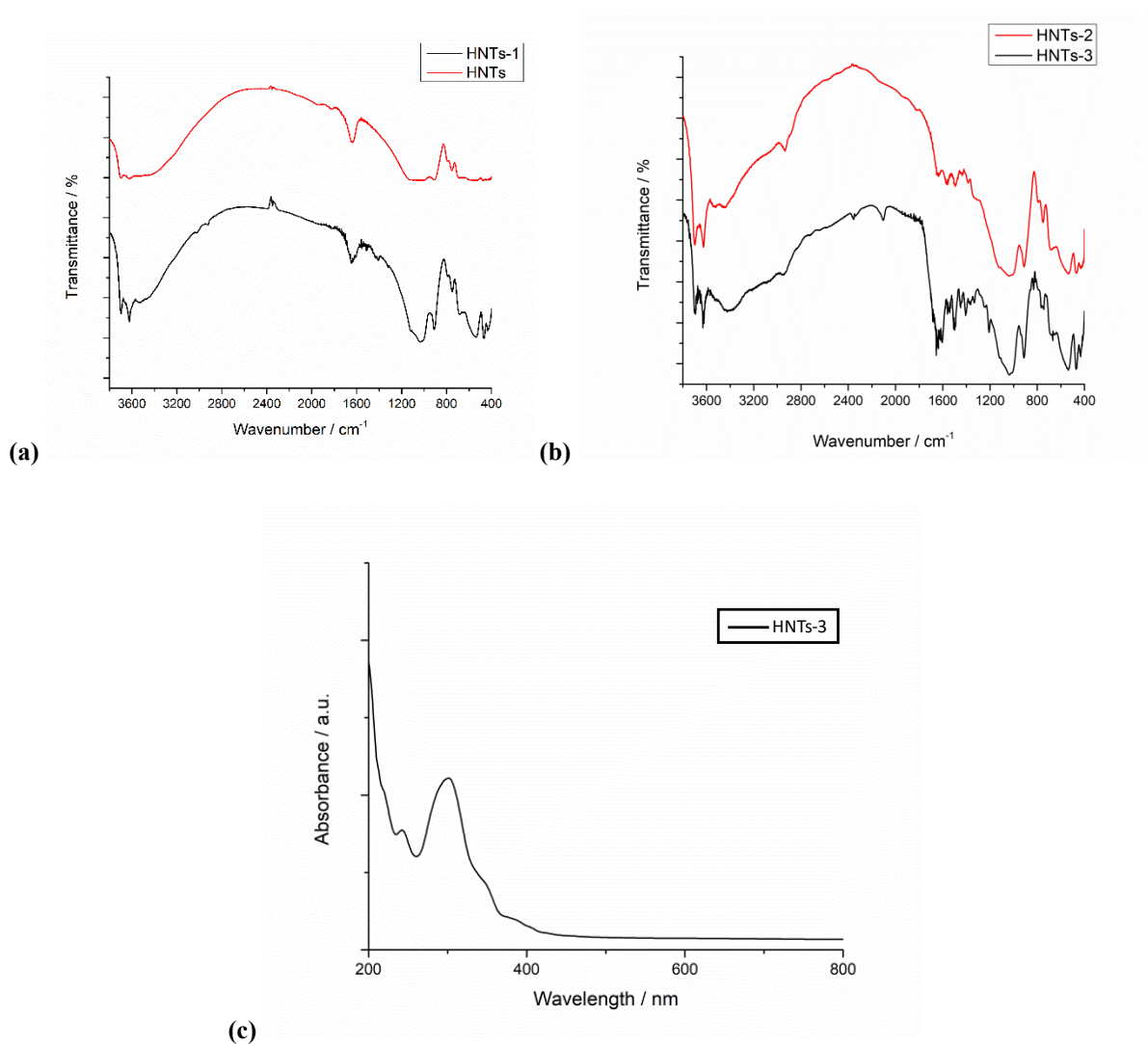


Figure 2. FT-IR spectra of (a) **HNTs-1** and pristine HNTs; (b) **HNTs-3** and **HNTs-2** nanomaterials; (c) UV-*vis* spectrum of an aqueous dispersion of **HNTs-3** nanomaterial ($[\text{HNTs-3}] = 0.123 \text{ mg mL}^{-1}$).

The UV-*vis* absorption spectrum of **HNTs-3** shows the successful grafting of drug molecules onto the HNTs surface (Figure 2c). As shown in Figure 2c, the aqueous dispersion of the nanomaterial exhibits the characteristic absorption of MTX at ca. 300 nm. On the contrary amino modified HNTs did not show any relevant absorption.

DLS experiments evidenced that the hydrodynamic diameter of **HNTs-3** is $650 \pm 74 \text{ nm}$, while its surface charge is still negative as evidenced by the ζ -potential ($-22 \pm 1.2 \text{ mV}$). This value is slight lower than that of pure HNTs (-20.7 mV)³⁵ in agreement to the presence of carboxyl groups from the MTX structure covalently linked on the external surface of the tubes.³⁶

TEM micrographies (Figure 3) clearly show the different morphologies of the nanomaterials obtained by the two different synthetic approaches. As it is possible to note from the Figure 3A, in the **HNTs-1** nanomaterial, HNTs lumens are barely observable further confirming the successful loading of MTX into HNTs interior. Conversely, the **HNTs-3** nanomaterial exhibits the characteristic hollow tubular structure of halloysite as a shell with an organic core (Figure 3B). In addition, we also observed the formation of some clusters onto the external surface of HNTs which could be due to supramolecular interactions between the different MTX units grafted on the HNTs surface as confirmed by EDS elemental mapping (Figure 3D). The EDS spectrum was also obtained by integration over the entire region and confirmed the presence of C and N atoms from the MTX grafted coating onto **HNTs-3** nanomaterial besides the Al, Si and O atoms related to the inorganic support (Figure 3C).

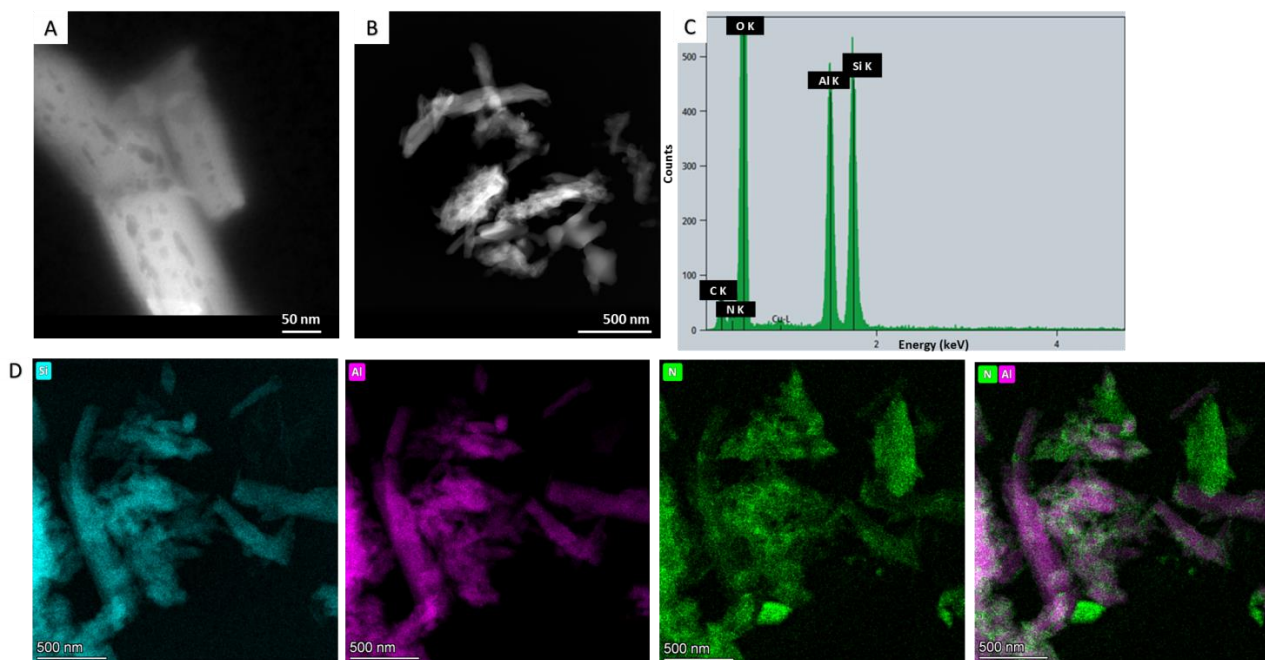
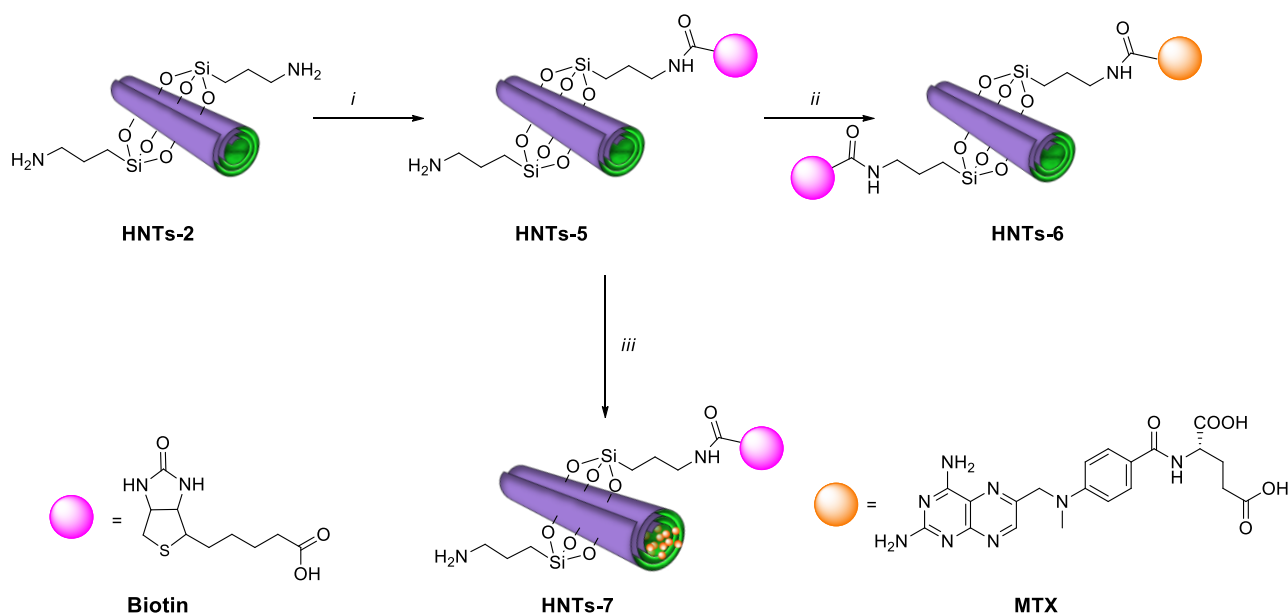


Figure 3. HAADF-STEM images of (A) **HNTs-1**; (B) **HNTs-3** and (C) selected EDX spectrum; (D) EDX elemental mapping images.

3.2. HNTs as drug delivery systems

Among the different targeting agents, recently, biotin has been widely used as a promising tumor targeting ligand²⁹ since its receptor is overexpressed in many cancer cells and could barely be

found in normal cells. Therefore, to enhance the active targeting effect toward cancer cells, we synthesized HNTs based nanomaterials bearing biotin units on their external surface (Scheme 2).



Scheme 2. Schematic representation of the synthesis of **HNTs-5**, **HNTs-6** and **HNTs-7** nanomaterials. Synthetic route: (i) biotin, EDC·HCl, DMF, 48 h, r.t., (ii) MTX, EDC·HCl, DMF, 48 h, r.t., (iii) MTX, H₂O, vacuum, 18 h, r.t..

Starting from **HNTs-2** nanomaterial, biotin units were covalently linked onto HNTs external surface by an EDC mediated condensation in DMF, at room temperature obtaining the **HNTs-5** nanomaterial which showed, as estimated by TGA, a percent loading of biotin onto HNTs of ca. 2.6 wt%, corresponding to a degree of functionalization of 0.11 mmol g⁻¹. Also in this case, based on the stoichiometric ratio between the -NH₂ groups in **HNTs-2** (0.6 mmol g⁻¹) and the biotin molecules in **HNTs-5** we estimated the presence of some unreacted amino groups still present on HNTs surface. Afterwards, in a second step, this nanomaterial was used for the covalent grafting of MTX, once again in the presence of EDC as coupling agent, affording the **HNTs-6** nanomaterial which showed a percent loading of MTX of ca. 4 wt% (Scheme 2). Conversely, the amide condensation between biotin and **HNTs-3** did not occur. Probably, the presence of MTX units onto HNTs external surface yield relevant steric hindrance which limits the -NH₂ groups accessibility. The **HNTs-5** nanomaterial was also used for the supramolecular loading of MTX into HNTs lumen

obtaining the final nanomaterial **HNTs-7**, which a percent loading of MTX of ca. 2 wt%, as estimated by TGA.

The **HNTs-5** and **HNTs-6** nanomaterials were characterized by TGA and FT-IR spectroscopy. Thermogravimetric results evidenced that both **HNTs-5** and **HNTs-6** possess larger ML150 values (4.91 and 4.81%, respectively) compared to that of **HNTs-2** (1.92%). We observed that **HNTs-5** presents lower MR700 values (80.1%) with respect to that of **HNTs-2** as a consequence of the covalent grafting of biotin on the halloysite outer surface. On the other hand, **HNTs-6** and **HNTs-7** presents a lower MR700 with respect to the mentioned nanomaterials due to the further loading of the MTX (Figure S1).

FT-IR spectra of **HNTs-5** and **HNTs-6** nanomaterials further confirm the successful modification of HNTs surface. Indeed, after the biotinylation reaction, the FT-IR spectra of **HNTs-5** nanomaterial present some additional bands, related to the typical vibrations of the biotin groups (Figure S2). The absence of any band at ca. 1800 cm^{-1} related to the presence of carboxylic groups further confirm the covalent linkage. The FT-IR spectrum of **HNTs-6** also showed the typical vibration bands of MTX. Similarly, the FT-IR spectrum of **HNTs-7** (data not shown) presents the vibration bands both of MTX and biotin

3.3 Kinetic release

To evaluate the performances of the synthesized nanomaterials for application in biomedical field, the kinetic release of MTX from **HNTs-1**, **HNTs-3**, and **HNTs-4** nanomaterials was evaluated by the dialysis bag method using conditions designed to mimic physiological conditions (HCl $1 \cdot 10^{-3}$ M and phosphate buffer pH 7.4) and the obtained kinetic data are shown in Figure 4. These nanomaterials were chosen as models to investigate the effect of HNTs functionalization on MTX release; indeed, we assumed that no interaction should occur between MTX and biotin in **HNTs-6** and **HNTs-7** and therefore the MTX release from them should be comparable to that obtained from **HNTs-1** (similar to **HNTs-7**) and **HNTs-3** (similar to **HNTs-6**).

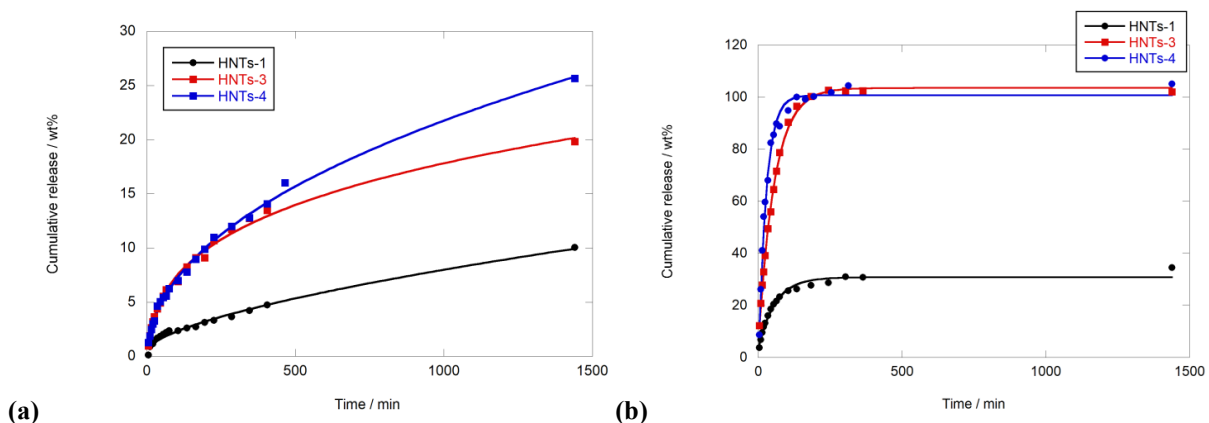


Figure 4. Kinetic release of MTX from **HNTs-1**, **HNTs-3** and, **HNTs-4** in (a) HCl $1 \cdot 10^{-3}$ M, pH 3.0; (b) phosphate buffer (0.05 M) solution at pH 7.4, at 37 °C.

As it is possible to observe from Figure 5, at pH 3.0, the MTX release from **HNTs-1**, **HNTs-3** and **HNTs-4**, was slow and sustained over the time (ca. 10 wt%, 20 wt% and 25 wt% of the total amount of MTX, respectively) released after 24 h. Conversely, at pH 7.4 a fast MTX release was observed in the first 300 min, after which a plateau is observed, in all cases. In detail, ca. 30 wt% of the total MTX loaded is released from **HNTs-1**, whereas the total amount of MTX loaded was released from **HNTs-3** and **HNTs-4**.

These significant differences between **HNTs-1** and **HNTs-3** or **HNTs-4**, at both pH, highlight the importance of functionalization, demonstrating its usefulness for the design of rational, modified drug delivery systems. Indeed, it is possible to observe that **HNTs-1** (supramolecular complex) retains the drug permanently at pH 7.4, not allowing total MTX release. This is a typical behavior of clay minerals, since they establish strong, non-specific drug adsorption that usually limits the amount of substance released, which subsequently jeopardizes drug therapeutic doses.

Furthermore, it is noticeable that the pH of the environment did not only influence the shape of the release profile but also the total amount of MTX released (higher at pH 7.4 than at pH 3.0). This result was attributable to the solubility of the drug in the release media. MTX possesses a $pK_{a1} = 4.8$ and $pK_{a2} = 5.5$, which means that it is highly ionized, with two negative charges, at pH 7.4 (higher solubility), leading to greater and faster dissolution and, subsequently, to a greater and faster release compared to pH 3.0.

We hypothesized that in both mediums, the hydrolysis of amide bond occurs in **HNTs-3** and **HNTs-4**; nonetheless, the MTX released molecules at pH 7.4 can spread through the dialysis membrane being limited at pH 3.0.

The kinetic data obtained were analyzed by a first order (Eq. 2) and Korsmeyer–Peppas (power law, Eq. 3) models to investigate more deeply the release behavior of MTX from all nanomaterials. The models were chosen since they are those commonly used to study the release of drugs from porous platforms.

$$M_t = M_0 e^{-kt} \quad (2)$$

$$\frac{M_t}{M_\infty} = at^n \quad (3)$$

For the first order model (Eq. 2), M_t is the amount of drug dissolved; M_0 is the amount of drug in the solution at time 0; k is the first order rate constant. For the power law (Eq. 3) M_t/M_∞ is the fractional release of the drug; the constant a depends on the structure and geometry of the platform; n is a release exponent related to the drug release mechanism. The obtained kinetic parameters are reported in Table 1. The results showed that, a pH 3.0, the kinetic data were better fitted by power law model (see R^2 values, Table 1).

In general, HNTs can be considered as porous systems with cylindrical geometry, whose n values are usually around 0.45. In this scenario, $n = 0.45$ (**HNTs-4**) and 0.27 (**HNTs-3**) correspond to Fickian diffusion, while for $0.45 < n < 1$ (**HNTs-1**) the diffusion will be classified as non-Fickian.³⁷ The n value of **HNTs-1** confirms the presence of MTX molecules within the lumen of halloysite, from which they can dissolve and diffuse. On the other hand, the covalent linkage of MTX molecules on the HNTs external surface explains the low n value of **HNTs-3**; in this case, indeed, the cylindrical geometry of halloysite did not influence the release process. Noteworthy, the n value obtained for **HNTs-4** (Table 1) could indicate that the release of MTX occurs both from the HNTs lumen and from the external surface.

At pH 7.4, the release of MTX follows the first order model in all cases investigated. The values of the first order release constants are in agreement with the release profiles (Figure 5b), **HNTs-4** being the fastest one, followed by **HNTs-3**.

Table 1. Kinetic parameters for MTX release from **HNTs-1**, **HNTs-3** and, **HNTs-4** at pH 3.0 and pH 7.4.

		First-order			Power Fit		
		M_{∞}	k	R^2	k	n	R^2
		(wt%)	(min ⁻¹)		(min ⁻¹)		
pH 3.0	HNTs-1	12.2±1.4	(9±2)·10 ⁻⁴	0.9762	0.09±0.03	0.64±0.4	0.9862
	HNTs-3	17.5±0.8	(2.8±0.2)·10 ⁻³	0.9829	3.4±0.6	0.27±0.02	0.9951
	HNTs-4	25.0±1.0	(1.7±0.2)·10 ⁻³	0.9875	1.0±0.1	0.45±0.02	0.9971
pH 7.4	HNTs-1	27±1	(1.72±0.02)·10 ⁻²	0.9789	n.a. ^a	n.a. ^a	n.a. ^a
	HNTs-3	99±1	(1.78±0.05)·10 ⁻²	0.9984	n.a. ^a	n.a. ^a	n.a. ^a
	HNTs-4	107±4	(3.60±0.02)·10 ⁻²	0.9907	n.a. ^a	n.a. ^a	n.a. ^a

^anot applicable

3.4 Biological properties

The cytotoxicity of the HNTs modified with MTX nanomaterials was tested by MTT assay on two different leukemia cell lines, being the MTX an antiproliferative drug administered in leukemias especially lymphoid type. For this purpose, we choose to test the nanomaterials on an acute myeloid leukemia cell line (HL-60) and on its multidrug resistant variant (HL-60R). The latter is a cell line that shows a multi-drug resistant phenotype and therefore constitutes an MDR study model on which to evaluate the cytotoxic action of new nanoformulations and compare it to that obtained on the corresponding sensitive line. The IC₅₀ values obtained for the synthesized nanomaterials are summarized in Table 2. It should be noted that these values were obtained by treating the cell lines with aqueous dispersion of HNTs nanomaterials; thus, a proper comparison with MTX could not be performed, because of its highly hydrophobic character. When MTX is solubilized in DMSO it showed IC₅₀ values of 4.6 ± 0.3 nM and 26.5 ± 12.1 nM for HL-60 and HL-60R cell lines, respectively.

As it is possible to note, the **HNTs-1** nanomaterial showed higher IC₅₀ value for both cell lines (entries 1 and 4) than those of **HNTs-3** and **HNTs-4** nanomaterials. These findings agree with the low availability of the MTX due to its strong interaction with halloysite lumen. Conversely, the

covalent linkage of MTX on the HNTs external surface as in **HNTs-3** (entries 2 and 5) is advantageous in improving the cytotoxicity of drug. The results obtained with **HNTs-4** (entries 3 and 6) confirmed that the cytotoxicity is mainly related to the MTX linked on the external HNTs surface.

Table 2. IC₅₀ values of the **HNTs-1**, **HNTs-3** and **HNTs-4** investigated on the different cell lines.

Entry	HNTs nanomaterials	IC ₅₀ (nM) ^a
	<i>HL60</i>	
1	HNTs-1	22.0 ± 13.8
2	HNTs-3	6.2 ± 1.9
3	HNTs-4	8.1 ± 0.2
	<i>HL60 R</i>	
4	HNTs-1	210.0 ± 21.2
5	HNTs-3	39.5 ± 15.2
6	HNTs-4	46.5 ± 0.7

^acell lines treated with aqueous dispersion of HNTs based nanomaterials.

After HNTs modification with biotin we obtained different results depending on the system investigated. **HNTs-6** nanomaterial showed higher IC₅₀ values for both cell lines (82.5 ± 1.8 nM and 385 ± 0.0 mM, for HL-60 and HL-60R, respectively) than those of unbiotinylated **HNTs-3**. These unexpected results could be in agreement with previous reported MTS test on the same cell lines.³⁸ It is indeed known that cellular uptake of complex nanoparticles is strictly correlated to the particle size, small particles showing higher cellular internalization, localization, and cytotoxicity with respect to the larger ones. The biotinylation of **HNTs-3** to give **HNTs-6** nanomaterial, increases the size of the system, as proved by DLS measurements, worsening the biological performances. It was indeed found that **HNTs-6** exhibited a hydrodynamic diameter of ca. 712 ±

117 nm, in agreement with the presence of different organic molecules present on HNTs surface with a ζ -potential equals to -25.3 ± 0.8 mV.

Finally, the cell viability following treatment with the biotinylated **HNTs-7** nanomaterials was drastically lower if compared with the unbiotinylated **HNTs-1** one, for both cell lines, indicating a crucial role of biotin units in determining the higher anticancer performance of the MTX carrier systems based on HNTs.

The IC_{50} value of the biotinylated sample indeed, was at least three times lower than that calculated for the unbiotinylated one for HL-60 cell lines ($IC_{50} = 6.0 \pm 0.0$ nM) while it was ca. seven times lower in the case of HL-60R ($IC_{50} = 29.8 \pm 10.0$ nM) and, in both cases comparable to the free drug in DMSO. These results could be explained by considering an increased internalization of the biotinylated **HNTs-7** nanomaterial into the cells *via* the receptor-mediated endocytosis, thus showing higher cytotoxicity in comparison to the unbiotinylated (**HNTs-1**) ones.²⁷ These results appear important as it would allow us to use the same systems as drug carriers to lead the antitumor drug and a target therapy, such as P-gp inhibitor for example, to MDR cells obtaining cytotoxic action comparable to that of sensitive cells.

4. Conclusions

HNTs represent one of the most emerging nanomaterials designed for their use in biomedicine. Their structural diversity, between external and internal surface, is a challenging for chemists in order to obtain "smart" nanomaterials able to carrier and delivery drug molecules in specific conditions and/or targets.

In this study both a prodrug approach, to obtain MTX based HNTs nanomaterials, and the development of specific systems, based on biotin, able to deliver MTX in target sites were carried out.

Firstly, we develop a synthetic strategy to link MTX molecules on HNTs surfaces to obtain the prodrug HNTs nanomaterials. To reach this goal different approaches were envisaged *i)* a supramolecular interaction between the HNTs and MTX (**HNTs-1**); *ii)* a covalent grafting of the drug onto the HNTs external surface (**HNTs-3**) and, *iii)* a combination of both approaches (**HNTs-4**). Successively, to reduce systemic toxic effects, to enhance the cellular uptake and to increase the therapeutic efficacy of the MTX in cancer cells, an active targeting system based on the surface receptor-mediated drug delivery system strategy was developed. Biotin was chosen as ligand, and

it was covalently linked to HNTs external surface (**HNTs-6** and **HNTs-7** s). The success of the functionalization was confirmed by the same techniques above reported. All HNTs nanomaterials were characterized by several techniques (FT-IR, TGA, UV-vis, DLS, ζ -potential and HAADF/STEM). Kinetic release experiments at different pH conditions (HCl solution $1 \cdot 10^{-3}$ M, pH 3.0; phosphate buffer solution 0.05 M, pH 7.4) at 37 °C were also performed.

Finally, as a proof-of-concept application of HNTs nanomaterials in cancer therapy, the cytotoxic effects of the multifunctional carriers were evaluated on acute myeloid leukemia cell lines, HL60 and its multidrug resistance variant, HL60-R. The obtained results showed that in the case of prodrug HNTs nanomaterials (**HNTs-3** and **4**) the covalent linkage of MTX on the HNTs external surface is advantageous in improving the cytotoxicity of drug molecules in both cell lines analyzed. In addition, the IC₅₀ values of the biotinylated sample (**HNTs-7**), was at least three times lower than that calculated for the unbiotinylated one for HL-60 while it was ca. seven times lower in the case of HL-60R.

The obtained results showed that both the MTX prodrug system and the biotinylated ones played a crucial role in the biological activity and, they are promising agents for the cancer treatments.

ACKNOWLEDGMENT

The work was carried out in the frame of the PON “AIM: Attrazione e Mobilità Internazionale” No. 1808223-1 project. Authors also thank financial support of Andalusian project P18-RT-3786.

REFERENCES

1. Crabtree, M. J.; Hale, A. B.; Channon, K. M., Dihydrofolate Reductase Protects Endothelial Nitric Oxide Synthase from Uncoupling in Tetrahydrobiopterin Deficiency. *Free Radical Biol. Med.* **2011**, 50 (11), 1639-1646.
2. Banerjee, D.; Mayer-Kuckuk, P.; Capiiaux, G.; Budak-Alpdogan, T.; Gorlick, R.; Bertino, J. R., Novel Aspects of Resistance to Drugs Targeted to Dihydrofolate Reductase and Thymidylate Synthase. *Biochimica et Biophysica Acta (BBA) - Molecular Basis of Disease* **2002**, 1587 (2), 164-173.
3. Lin, J.; Li, Y.; Li, Y.; Cui, F.; Yu, F.; Wu, H.; Xie, L.; Luo, F.; Hou, Z.; Lin, C., Self-Targeted, Bacillus-Shaped, and Controlled-Release Methotrexate Prodrug Polymeric Nanoparticles for Intratumoral Administration with Improved Therapeutic Efficacy in Tumor-Bearing Mice. *J. Mater. Chem. B* **2015**, 3 (39), 7707-7717.
4. Ma, H.; He, C.; Cheng, Y.; Yang, Z.; Zang, J.; Liu, J.; Chen, X., Localized Co-Delivery of Doxorubicin, Cisplatin, and Methotrexate by Thermosensitive Hydrogels for Enhanced Osteosarcoma Treatment. *ACS Applied Materials & Interfaces* **2015**, 7 (49), 27040-27048.

5. Muthukumar, T.; Prabhavathi, S.; Chamundeeswari, M.; Sastry, T. P., Bio-Modified Carbon Nanoparticles Loaded with Methotrexate Possible Carrier for Anticancer Drug Delivery. *Materials Science and Engineering: C* **2014**, *36*, 14-19.
6. Jornada, D. H.; Dos Santos Fernandes, G. F.; Chiba, D. E.; De Melo, T. R. F.; Dos Santos, J. L.; Chung, M. C., The Prodrug Approach: A Successful Tool for Improving Drug Solubility. *Molecules* **2016**, *21* (1), 42.
7. Mahesh, S.; Tang, K.-C.; Raj, M., Amide Bond Activation of Biological Molecules. *Molecules* **2018**, *23* (10), 2615.
8. Peixoto, D.; Pereira, I.; Pereira-Silva, M.; Veiga, F.; Hamblin, M. R.; Lvov, Y.; Liu, M.; Paiva-Santos, A. C., Emerging Role of Nanoclays in Cancer Research, Diagnosis, and Therapy. *Coord. Chem. Rev.* **2021**, *440*, 213956.
9. Liu, M.; Jia, Z.; Jia, D.; Zhou, C., Recent Advance in Research on Halloysite Nanotubes-Polymer Nanocomposite. *Prog. Polym. Sci.* **2014**, *39* (8), 1498-1525.
10. Fakhrullina, G. I.; Akhatova, F. S.; Lvov, Y. M.; Fakhrullin, R. F., Toxicity of Halloysite Clay Nanotubes in Vivo: A Caenorhabditis Elegans Study. *Environm. Sci. Nano* **2015**, *2* (1), 54-59.
11. Kryuchkova, M.; Danilushkina, A.; Lvov, Y.; Fakhrullin, R., Evaluation of Toxicity of Nanoclays and Graphene Oxide in Vivo: A Paramecium Caudatum Study. *Environm. Sci. Nano* **2016**, *3* (2), 442-452.
12. Bellani, L.; Giorgetti, L.; Riela, S.; Lazzara, G.; Scialabba, A.; Massaro, M., Ecotoxicity of Halloysite Nanotube-Supported Palladium Nanoparticles in Raphanus Sativus L. *Environ. Toxicol. Chem.* **2016**, *35* (10), 2503-2510.
13. Bretti, C.; Cataldo, S.; Gianguzza, A.; Lando, G.; Lazzara, G.; Pettignano, A.; Sammartano, S., Thermodynamics of Proton Binding of Halloysite Nanotubes. *J. Phys. Chem. C* **2016**, *120* (14), 7849-7859.
14. Stavitskaya, A. V.; Novikov, A. A.; Kotelev, M. S.; Kopitsyn, D. S.; Rozhina, E. V.; Ishmukhametov, I. R.; Fakhrullin, R. F.; Ivanov, E. V.; Lvov, Y. M.; Vinokurov, V. A., Fluorescence and Cytotoxicity of Cadmium Sulfide Quantum Dots Stabilized on Clay Nanotubes. *Nanomaterials* **2018**, *8* (6), 391.
15. Massaro, M.; Noto, R.; Riela, S., Past, Present and Future Perspectives on Halloysite Clay Minerals. *Molecules* **2020**, *25* (20).
16. Massaro, M.; Campofelice, A.; Colletti, C. G.; Lazzara, G.; Noto, R.; Riela, S., Functionalized Halloysite Nanotubes: Efficient Carrier Systems for Antifungine Drugs. *Appl. Clay Sci.* **2018**, *160*, 186-192.
17. Massaro, M.; Casiello, M.; D'Accolti, L.; Lazzara, G.; Nacci, A.; Nicotra, G.; Noto, R.; Pettignano, A.; Spinella, C.; Riela, S., One-Pot Synthesis of ZnO Nanoparticles Supported on Halloysite Nanotubes for Catalytic Applications. *Appl. Clay Sci.* **2020**, *189*.
18. Lin, T.; Zhao, S.; Niu, S.; Lyu, Z.; Han, K.; Hu, X., Halloysite Nanotube Functionalized with La-Ca Bimetallic Oxides as Novel Transesterification Catalyst for Biodiesel Production with Molecular Simulation. *Energy Convers. Manage.* **2020**, *220*.
19. Stavitskaya, A. V.; Kozlova, E. A.; Kurenkova, A. Y.; Glotov, A. P.; Selischev, D. S.; Ivanov, E. V.; Kozlov, D. V.; Vinokurov, V. A.; Fakhrullin, R. F.; Lvov, Y. M., Ru/Cds Quantum Dots Templated on Clay Nanotubes as Visible-Light-Active Photocatalysts: Optimization of S/Cd Ratio and Ru Content. *Chemistry – A European Journal* **2020**, *26* (57), 13085-13092.

20. Laura Alfieri, M.; Massaro, M.; d'Ischia, M.; D'Errico, G.; Gallucci, N.; Gruttadauria, M.; Licciardi, M.; Liotta, L. F.; Nicotra, G.; Sfuncia, G.; Riela, S., Site-Specific Halloysite Functionalization by Polydopamine: A New Synthetic Route for Potential near Infrared-Activated Delivery System. *J. Colloid Interface Sci.* **2021**.
21. Lvov, Y.; Aerov, A.; Fakhrullin, R., Clay Nanotube Encapsulation for Functional Biocomposites. *Adv. Colloid Interface Sci.* **2014**, *207*, 189-198.
22. Riela, S.; Barattucci, A.; Barreca, D.; Campagna, S.; Cavallaro, G.; Lazzara, G.; Massaro, M.; Pizzolanti, G.; Salerno, T. M. G.; Bonaccorsi, P.; Puntoriero, F., Boosting the Properties of a Fluorescent Dye by Encapsulation into Halloysite Nanotubes. *Dyes Pigm.* **2021**, *187*.
23. Massaro, M.; Barone, G.; Biddecì, G.; Cavallaro, G.; Di Blasi, F.; Lazzara, G.; Nicotra, G.; Spinella, C.; Spinelli, G.; Riela, S., Halloysite Nanotubes-Carbon Dots Hybrids Multifunctional Nanocarrier with Positive Cell Target Ability as a Potential Non-Viral Vector for Oral Gene Therapy. *J. Colloid Interface Sci.* **2019**, *552*, 236-246.
24. Massaro, M.; Amorati, R.; Cavallaro, G.; Guernelli, S.; Lazzara, G.; Milioto, S.; Noto, R.; Poma, P.; Riela, S., Direct Chemical Grafted Curcumin on Halloysite Nanotubes as Dual-Responsive Prodrug for Pharmacological Applications. *Colloids Surf. B. Biointerfaces* **2016**, *140*, 505-513.
25. Kunjiappan, S.; Pavadai, P.; Vellaichamy, S.; Ram Kumar Pandian, S.; Ravishankar, V.; Palanisamy, P.; Govindaraj, S.; Srinivasan, G.; Premanand, A.; Sankaranarayanan, M.; Theivendren, P., Surface Receptor-Mediated Targeted Drug Delivery Systems for Enhanced Cancer Treatment: A State-of-the-Art Review. *Drug Dev. Res.* **2021**, *82* (3), 309-340.
26. Yang, W.; Wang, M.; Ma, L.; Li, H.; Huang, L., Synthesis and Characterization of Biotin Modified Cholesteryl Pullulan as a Novel Anticancer Drug Carrier. *Carbohydr. Polym.* **2014**, *99*, 720-727.
27. Shi, H.; Liang, N.; Liu, J.; Li, S.; Gong, X.; Yan, P.; Sun, S., Aie-Active Polymeric Micelles Based on Modified Chitosan for Bioimaging-Guided Targeted Delivery and Controlled Release of Paclitaxel. *Carbohydr. Polym.* **2021**, *269*, 118327.
28. Doerflinger, A.; Quang, N. N.; Gravel, E.; Pinna, G.; Vandamme, M.; Ducongé, F.; Doris, E., Biotin-Functionalized Targeted Polydiacetylene Micelles. *Chem. Commun.* **2018**, *54* (29), 3613-3616.
29. Ren, W. X.; Han, J.; Uhm, S.; Jang, Y. J.; Kang, C.; Kim, J.-H.; Kim, J. S., Recent Development of Biotin Conjugation in Biological Imaging, Sensing, and Target Delivery. *Chem. Commun.* **2015**, *51* (52), 10403-10418.
30. Luo, Y.; Humayun, A.; Murray, T. A.; Kemp, B. S.; McFarland, A.; Liu, X.; Mills, D. K., Cellular Analysis and Chemotherapeutic Potential of a Bi-Functionalized Halloysite Nanotube. *Pharmaceutics* **2020**, *12* (10), 962.
31. Labbozzetta, M.; Notarbartolo, M.; Poma, P., Can Nf-Kb Be Considered a Valid Drug Target in Neoplastic Diseases? Our Point of View. *International Journal of Molecular Sciences* **2020**, *21* (9), 3070.
32. Massaro, M.; Colletti, C. G.; Guernelli, S.; Lazzara, G.; Liu, M.; Nicotra, G.; Noto, R.; Parisi, F.; Pibiri, I.; Spinella, C.; Riela, S., Photoluminescent Hybrid Nanomaterials from Modified Halloysite Nanotubes. *J. Mater. Chem. C* **2018**, *6* (27), 7377-7384.
33. Poma, P.; Labbozzetta, M.; Zito, P.; Alduina, R.; Ramarosandratana, A. V.; Bruno, M.; Rosselli, S.; Sajeve, M.; Notarbartolo, M., Essential Oil Composition of *Alluaudia Procera* and in Vitro Biological Activity on Two Drug-Resistant Models. *Molecules* **2019**, *24* (16), 2871.

34. Ayyappan, S.; Sundaraganesan, N.; Aroulmoji, V.; Murano, E.; Sebastian, S., Molecular Structure, Vibrational Spectra and Dft Molecular Orbital Calculations (Td-Dft and Nmr) of the Antiproliferative Drug Methotrexate. *Spectrochimica Acta Part A: Molecular and Biomolecular Spectroscopy* **2010**, *77* (1), 264-275.
35. Cavallaro, G.; Chiappisi, L.; Pasbakhsh, P.; Gradzielski, M.; Lazzara, G., A Structural Comparison of Halloysite Nanotubes of Different Origin by Small-Angle Neutron Scattering (Sans) and Electric Birefringence. *Appl. Clay Sci.* **2018**, *160*, 71-80.
36. Voicu, A. I.; Gârea, S. A.; Ghebaur, A.; Nistor, C. L.; Sârbu, A.; Vasile, E.; Mitran, R.; Iovu, H., New Nanocarriers Based on Porous Clay Heterostructures (Pch) Designed for Methotrexate Delivery. *Microporous Mesoporous Mater.* **2021**, *328*, 111434.
37. Ritger, P. L.; Peppas, N. A., A Simple Equation for Description of Solute Release I. Fickian and Non-Fickian Release from Non-Swellable Devices in the Form of Slabs, Spheres, Cylinders or Discs. *J. Controlled Release* **1987**, *5* (1), 23-36.
38. Massaro, M.; Poma, P.; Colletti, C. G.; Barattucci, A.; Bonaccorsi, P. M.; Lazzara, G.; Nicotra, G.; Parisi, F.; Salerno, T. M. G.; Spinella, C.; Riela, S., Chemical and Biological Evaluation of Cross-Linked Halloysite-Curcumin Derivatives. *Appl. Clay Sci.* **2020**, *184*.